

# UC San Diego

## UC San Diego Previously Published Works

### Title

The Caenorhabditis elegans RIG-I Homolog DRH-1 Mediates the Intracellular Pathogen Response upon Viral Infection

### Permalink

<https://escholarship.org/uc/item/2bj8h6qg>

### Journal

Journal of Virology, 94(2)

### ISSN

0022-538X

### Authors

Sowa, Jessica N

Jiang, Hongbing

Somasundaram, Lakshmi

et al.

### Publication Date

2020-01-06


### DOI

10.1128/jvi.01173-19

Peer reviewed



# The *Caenorhabditis elegans* RIG-I Homolog DRH-1 Mediates the Intracellular Pathogen Response upon Viral Infection

Jessica N. Sowa,<sup>a</sup> Hongbing Jiang,<sup>b,c</sup> Lakshmi Somasundaram,<sup>a</sup> Eillen Teclé,<sup>a</sup> Guorong Xu,<sup>d</sup> David Wang,<sup>b,c</sup>  
 Emily R. Troemel<sup>a</sup>

<sup>a</sup>Division of Biological Sciences, University of California, San Diego, La Jolla, California, USA

<sup>b</sup>Department of Molecular Microbiology, Washington University in St. Louis School of Medicine, St. Louis, Missouri, USA

<sup>c</sup>Department of Pathology and Immunology, Washington University in St. Louis School of Medicine, St. Louis, Missouri, USA

<sup>d</sup>Center for Computational Biology and Bioinformatics, Department of Medicine, University of California, San Diego, La Jolla, California, USA

**ABSTRACT** Mammalian retinoic acid-inducible gene I (RIG-I)-like receptors detect viral double-stranded RNA (dsRNA) and 5'-triphosphorylated RNA to activate the transcription of interferon genes and promote antiviral defense. The *Caenorhabditis elegans* RIG-I-like receptor DRH-1 promotes defense through antiviral RNA interference (RNAi), but less is known about its role in regulating transcription. Here, we describe a role for DRH-1 in directing a transcriptional response in *C. elegans* called the intracellular pathogen response (IPR), which is associated with increased pathogen resistance. The IPR includes a set of genes induced by diverse stimuli, including intracellular infection and proteotoxic stress. Previous work suggested that the proteotoxic stress caused by intracellular infections might be the common trigger of the IPR, but here, we demonstrate that different stimuli act through distinct pathways. Specifically, we demonstrate that DRH-1/RIG-I is required for inducing the IPR in response to Orsay virus infection but not in response to other triggers like microsporidian infection or proteotoxic stress. Furthermore, DRH-1 appears to be acting independently of its known role in RNAi. Interestingly, expression of the replication-competent Orsay virus RNA1 segment alone is sufficient to induce most of the IPR genes in a manner dependent on RNA-dependent RNA polymerase activity and on DRH-1. Altogether, these results suggest that DRH-1 is a pattern recognition receptor that detects viral replication products to activate the IPR stress/immune program in *C. elegans*.

**IMPORTANCE** *C. elegans* lacks homologs of most mammalian pattern recognition receptors, and how nematodes detect pathogens is poorly understood. We show that the *C. elegans* RIG-I homolog DRH-1 mediates the induction of the intracellular pathogen response (IPR), a novel transcriptional defense program, in response to infection by the natural *C. elegans* viral pathogen Orsay virus. DRH-1 appears to act as a pattern recognition receptor to induce the IPR transcriptional defense program by sensing the products of viral RNA-dependent RNA polymerase activity. Interestingly, this signaling role of DRH-1 is separable from its previously known role in antiviral RNAi. In addition, we show that there are multiple host pathways for inducing the IPR, shedding light on the regulation of this novel transcriptional immune response.

**KEYWORDS** *C. elegans*, innate immunity, plus-strand RNA virus

Retinoic acid-inducible gene I (RIG-I)-like receptors (RLRs) are an ancient family of cytoplasmic pattern recognition receptors that detect viral double-stranded RNA (dsRNA) and 5'-triphosphorylated RNA to trigger antiviral immune responses (1, 2). In mammals, this family includes RIG-I and MDA5, which contain a common N-terminal tandem caspase activation and recruitment domain (2CARD), a central DExD/H box motif helicase domain, and a zinc-binding C-terminal domain (CTD) (3). After the

**Citation** Sowa JN, Jiang H, Somasundaram L, Teclé E, Xu G, Wang D, Troemel ER. 2020. The *Caenorhabditis elegans* RIG-I homolog DRH-1 mediates the intracellular pathogen response upon viral infection. *J Virol* 94:e01173-19. <https://doi.org/10.1128/JVI.01173-19>.

**Editor** Julie K. Pfeiffer, University of Texas Southwestern Medical Center

**Copyright** © 2020 American Society for Microbiology. All Rights Reserved.

Address correspondence to Emily R. Troemel, [etroemel@ucsd.edu](mailto:etroemel@ucsd.edu).

**Received** 16 July 2019

**Accepted** 4 October 2019

**Accepted manuscript posted online** 16 October 2019

**Published** 6 January 2020

helicase and CTD bind to viral RNAs, these receptors trigger a signaling cascade via interaction of the CARD domain with the mitochondrial activator of virus signaling (MAVS) protein, which ultimately results in the activation of the interferon regulatory factor 3 (IRF3) and NF- $\kappa$ B transcription factors (4). These transcription factors trigger downstream defense gene expression, including an IRF3-mediated antiviral type I interferon response (5). Given the importance of RLRs in antiviral defense and autoimmunity, further understanding their evolution and signaling mechanisms in different contexts could provide new avenues for treatment of viral infections and autoimmune diseases.

RIG-I is one of the few pattern recognition receptors conserved between mammals and the model nematode *Caenorhabditis elegans*. Notably, *C. elegans* lacks the cytoplasmic pattern recognition receptors cGAS-STING and nucleotide-binding domain and leucine-rich repeat containing gene family (NLR) proteins and also lacks canonical Toll-like receptor/NF- $\kappa$ B signaling (6–9). Furthermore, *C. elegans* lacks obvious homologs of IRF3 and MAVS as well as interferon ligands and receptors. However, *C. elegans* possesses three genes that encode RIG-I-like receptor homologs: dicer-related helicases 1, 2, and 3 (*drh-1*, *drh-2*, and *drh-3*) (10, 11). Like RIG-I and MDA5, these genes encode a helicase domain and CTD but have a divergent N-terminal domain. DRH-1 was originally identified in *C. elegans* as a protein that interacts with the dsRNA-binding protein RDE-4 and Dicer/DCR-1 to process dsRNA into small interfering RNAs (siRNAs) (11). Subsequently, DRH-1 was found to mediate an antiviral response to several types of viral infection in *C. elegans* (12–16). Functional analysis indicated that the helicase domain from human RIG-I could replace the helicase domain in *C. elegans drh-1* to promote antiviral defense against a viral replicon and natural infection by Orsay virus (15). Interestingly, a small deletion in the CTD of DRH-1 was shown to underlie natural variation in *C. elegans* strains susceptible to infection by Orsay virus (12). Orsay virus has a positive-sense single-stranded RNA (ssRNA) genome composed of just two segments, the RNA1 segment, which contains an open reading frame (ORF) encoding an RNA-dependent RNA polymerase (RDRP), and the RNA2 segment, which contains an ORF encoding a capsid protein and an ORF implicated in viral exit (17, 18). Because *C. elegans* lacks interferon signaling, characterization of the antiviral mechanism of DRH-1 has focused on its role in mediating antiviral RNA interference (RNAi). The role for DRH-1 in triggering a transcriptional response to viral infection has been less clear (19).

Intriguingly, *C. elegans* responds to Orsay virus infection by upregulating the mRNA expression of a set of genes that are also induced during infection with pathogens in the microsporidian phylum (20–22). Like viruses, microsporidia are obligate intracellular pathogens that are natural pathogens of the *C. elegans* intestine (23). However, microsporidia are molecularly distinct, as they are eukaryotic pathogens in the fungal kingdom. We have named the common transcriptional response to microsporidia and Orsay virus the intracellular pathogen response (IPR), as it appears to represent a novel stress/immune pathway including many genes upregulated in the intestine (20, 24). The IPR is regulated by two members of the *pals* gene family, which is named for a protein signature of unknown biochemical function and has a single member each in mouse and human (24, 25). *C. elegans* mutants defective in the *pals-22* gene constitutively express IPR genes and have increased resistance to virus and microsporidian infection, which is reversed when increased IPR gene expression is suppressed by mutations in *pals-25* (22). In addition to increased pathogen resistance, *pals-22* mutants have several other phenotypes, including increased thermotolerance dependent on ubiquitin ligase components, increased RNAi, increased susceptibility to the extracellular bacterial pathogen *Pseudomonas aeruginosa*, slowed development, and shortened life span (24, 25). Thus, the activation of IPR genes is associated with a broad rewiring of *C. elegans* physiology.

How are IPR genes induced? Given that they can be induced not just by infection but also by proteotoxic stressors, like prolonged heat stress and proteasome blockade, a simple hypothesis was that intracellular infections by microsporidia and virus were creating proteotoxic stress that led to IPR gene induction (20). However, here, we show

that there are additional layers of complexity in the regulation of IPR induction. Specifically, we show that induction of IPR gene expression by viral infection requires the DRH-1 receptor. *drh-1* mutants are defective in inducing IPR genes in response to viral infection but not in response to other IPR triggers, including microsporidian infection and proteotoxic stress. Furthermore, we show that the activation of this transcriptional response does not require the known DRH-1-interacting proteins RDE-4 or DCR-1 and thus appears to occur via a mechanism that is distinct from the antiviral RNAi pathway. Finally, we use transcriptome sequencing (RNA-seq) to show that the IPR transcriptional program can be induced by ectopic expression of the Orsay virus RNA1 segment, and this induction depends on RDRP activity and on DRH-1. Together, these results suggest that DRH-1 acts a pattern recognition receptor in *C. elegans* to sense viral replication products and activate the IPR stress/immune program.

(This article was submitted to an online preprint archive [26].)

## RESULTS

**The RIG-I ortholog DRH-1 is required for induction of the intracellular pathogen response by Orsay virus infection but not by other stressors.** Infection of *C. elegans* by Orsay virus or by the microsporidian species *Nematocida parisii* induces a common set of genes as part of the IPR, including the gene *pals-5*. While the *pals-5* gene is of unknown function, the *pals-5p::GFP* reporter provides a convenient readout for the IPR (20). To investigate the role of DRH-1 in inducing the IPR, we examined *pals-5p::GFP* expression in the background of a *drh-1(ok3495)* partial-deletion allele. The *ok3495* allele contains a small (583-bp) in-frame deletion in what appears to be the helicase domain of *drh-1* (12). We found that, in contrast to wild-type animals, Orsay virus infection did not induce *pals-5p::GFP* reporter expression in *drh-1(ok3495)* mutants, despite these mutants carrying a higher viral load as assessed by reverse transcription-quantitative PCR (qRT-PCR) of the viral RNA1 genome segment (Fig. 1A to C). Because the *drh-1(ok3495)* allele is only a partial deletion, we used CRISPR/Cas9 editing to generate an additional deletion allele of *drh-1*, in which the entire genomic locus was removed (Fig. 1D). This complete-deletion allele, *drh-1(jy110)*, also failed to upregulate the IPR reporter when infected with Orsay virus (Fig. 1E) and carried a higher viral load than wild-type (*WT*) worms (Fig. 1F). For simplicity, from this point onward, the *drh-1(ok3495)* allele is denoted *drh-1(-)*.

Interestingly, we found no defect in IPR reporter activation by *N. parisii* infection or proteasome blockade in either of the *drh-1* mutant alleles (Fig. 2A to F). Additionally, we observed a very small difference in the *N. parisii* pathogen load in *drh-1(-)* mutants compared to *WT* controls and no difference in pathogen load in *drh-1(jy110)* mutants versus *WT* controls (Fig. 2B and D). Although the pathogen load difference in *drh-1(-)* mutants is statistically significant because of the large number ( $n > 5,000$ ), it may not be biologically relevant given the small difference in the means (0.1776 versus 0.1549). In both *drh-1* deletion alleles, proteasome blockade or *N. parisii* infection resulted in stronger green fluorescent protein (GFP) reporter activation than was seen in *WT* controls, with the effect being stronger in the *drh-1(jy110)* complete-deletion background (Fig. 2A to F). We also saw robust activation by prolonged heat stress in both *drh-1* mutant alleles (Fig. 2G and H). Furthermore, the increased *pals-5p::GFP* expression seen in the *pals-22* mutant background was not compromised by a mutation in *drh-1* (Fig. 2I), indicating that this pathway for IPR induction is not dependent on *drh-1*. Thus, we found that DRH-1 is required specifically for *pals-5p::GFP* expression in response to viral infection but not for the response to other triggers of *pals-5p::GFP* expression.

**DRH-1 acts independently of known RNAi factors to induce IPR mRNA expression in response to Orsay virus infection.** To obtain a broader picture of the requirement for DRH-1 in IPR gene expression, we performed qRT-PCR analysis of a panel of IPR genes, including those of unknown biochemical function, *pals-5* and *F26F2.1*; the mRNA-decapping enzyme-encoding gene *eol-1*; and the ubiquitin ligase complex component *skr-5* (20, 22, 24). As a negative control, we included *skr-1*, which is a ubiquitin ligase complex component that is not induced upon infection (20, 22, 24).

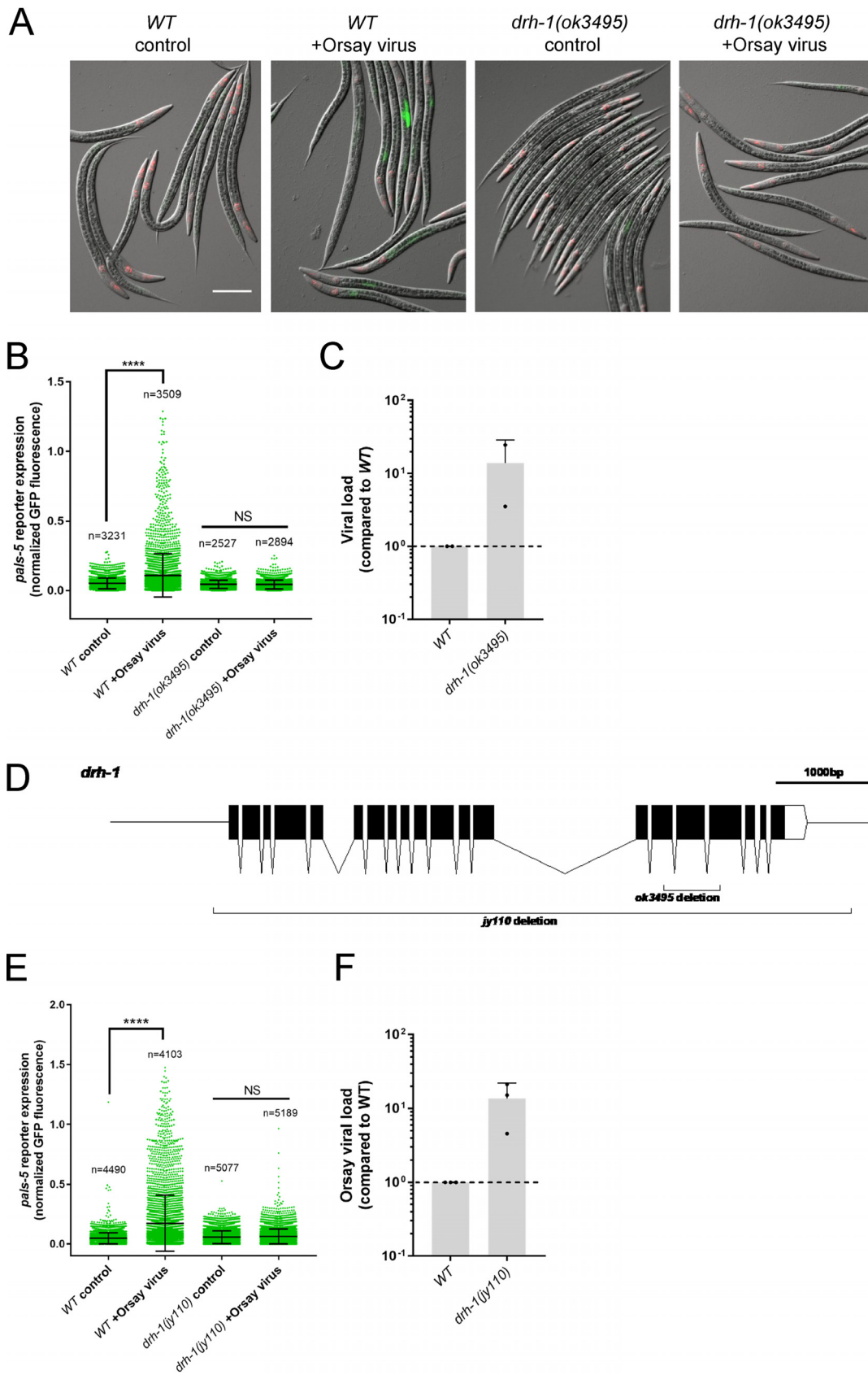


**FIG 1** DRH-1 is required for induction of the *pals-5p::GFP* IPR reporter upon viral infection. (A) *pals-5p::GFP* IPR reporter fluorescence after Orsay virus infection in WT versus *drh-1(ok3495)* backgrounds. Worms were infected with Orsay virus as L1 (Continued on next page)

We compared expression levels in Orsay virus-infected worms versus mock-infected controls at 12 h and 24 h postinfection (hpi) in *WT* and *drh-1(-)* mutant backgrounds (Fig. 3). We observed that at 12 hpi, there was a >10-fold induction of *pals-5*, *F26F2.1*, and *eol-1* in the Orsay virus-infected *WT* worms but no detectable induction in the *drh-1(-)* background (Fig. 3A), despite the fact that they were carrying a much higher viral load than their *WT* counterparts (Fig. 3B). We observed a similar pattern at 24 hpi, with *pals-5*, *F26F2.1*, and *eol-1* being induced >100-fold by Orsay virus infection in the *WT* background, while much less induction was seen in the *drh-1(-)* background despite *drh-1(-)* worms carrying an increased viral load (Fig. 3C and D). Although upregulation of IPR genes was observed in all three independent experiments at both 12 and 24 hpi, the magnitude of the induction varied between trials, as did the viral load (Fig. 3A to F). No induction of *skr-1* was observed in *WT* or *drh-1(-)* worms at 12 hpi or 24 hpi (Fig. 3A and C). In contrast to the lack of IPR induction in *drh-1* mutants at 12 hpi, some induction of *pals-5*, *F26F2.1*, and *eol-1* was observed in the *drh-1* mutant background at 24 hpi, raising the possibility that there could be a *drh-1*-independent induction of IPR genes by Orsay virus that functions at later stages of infection or with higher viral loads. Of note, at 24 hpi, *skr-5* showed higher expression levels in the infected *drh-1* mutants than in infected *WT* worms (Fig. 3C and E), demonstrating that unlike the other IPR genes assayed, *skr-5* induction does not require DRH-1. Analysis of the *drh-1(jy110)* full-deletion allele at 24 hpi confirmed these findings (Fig. 3E and F). Together, these data demonstrate that DRH-1 is required to induce several IPR genes in response to Orsay virus infection.

We next investigated whether other components of the antiviral RNAi pathway play a role in the virus-induced activation of IPR gene expression. In addition to *drh-1*, the *C. elegans* genome harbors two other DExD/H box RNA helicases with homology to mammalian RLRs, *drh-2* and *drh-3* (10, 11). DRH-2 is not thought to have a direct role in antiviral RNAi, but DRH-3 participates in the production of secondary siRNAs (15, 16). Other factors involved in the production of siRNAs targeting viral transcripts include RDE-4 and DCR-1, both of which interact directly with DRH-1, potentially as part of the complex that binds viral dsRNAs to initiate cleavage, and RDE-1, an argonaute that binds primary siRNAs (10, 11, 27, 28). To test the role of these genes, we infected *rde-1*, *rde-4*, *drh-2*, and *drh-3* mutants with Orsay virus for 12 and 24 h [infections were performed in parallel with the *WT* and *drh-1(-)* infections described above]. qRT-PCR analysis of a panel of IPR genes showed that none of these other antiviral RNAi mutants had impaired upregulation of IPR gene expression in response to viral infection (Fig. 3A and C). At both 12 and 24 hpi, IPR gene expression levels were generally higher in *rde-1*, *rde-4*, and *drh-3* mutants than in *WT* worms, which is consistent with the higher viral load observed in these mutants (Fig. 3B and D). No defects in IPR activation were observed in *drh-2* mutants, and they showed viral loads comparable to those of *WT* worms at both time points (Fig. 3A to D).

Because null mutations in the *C. elegans* Dicer homolog *dcr-1* lead to sterility or lethality (29), we used RNAi knockdown to determine whether *dcr-1* was required for

#### FIG 1 Legend (Continued)

larvae and imaged at 24 hpi. Bar = 100  $\mu$ m. (B) *pals-5p::GFP* IPR reporter fluorescence after Orsay virus infection in *WT* versus *drh-1(ok3495)* backgrounds. Worms were infected with Orsay virus as L2 larvae, and reporter expression was assayed at 24 hpi; each dot represents an individual animal. The graph shows combined results of three independent experimental replicates, with total numbers indicated. (C) qRT-PCR analysis of Orsay viral loads of samples from panel B. The graph shows combined results of two independent experimental replicates; each replicate is indicated as a dot, with columns representing combined means. Error bars represent standard deviations (SD). (D) Genomic locations of *jy110* and *ok3495* deletions in *drh-1*. (E) *pals-5p::GFP* IPR reporter fluorescence after Orsay virus infection in *WT* versus *drh-1(jy110)* backgrounds. Worms were infected with Orsay virus as L2 larvae, and reporter expression was assayed at 24 hpi; each dot represents an individual animal. The graph shows combined results of three independent experimental replicates, with total numbers indicated. (F) qRT-PCR analysis of Orsay viral loads of samples from panel E. The graph shows combined results of three independent experimental replicates; each replicate is indicated as a dot, with columns representing combined means. Error bars represent SD. For panels B and E, green fluorescence and length of animals were measured for ~1,000 individual animals per experimental replicate using a Copas Biosorter instrument. Means were compared using one-way ANOVA with Bonferroni correction. NS, not significant; \*\*\*\*,  $P < 0.0001$ .

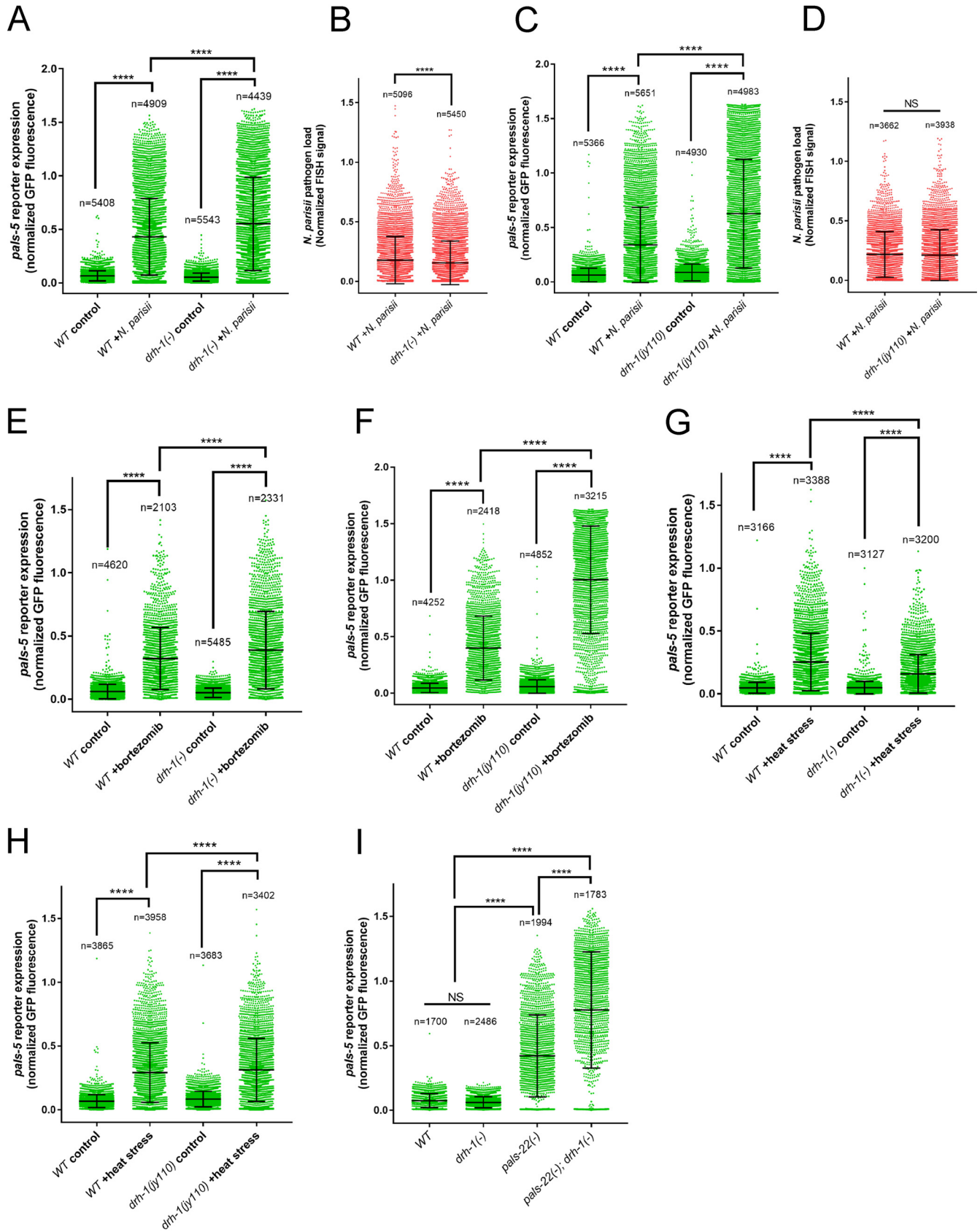


**FIG 2** DRH-1 is not required for induction of the *pals-5p::GFP* IPR reporter upon nonviral triggers. (A and C) *pals-5p::GFP* reporter fluorescence during *N. parisi* infection. Animals were infected with *N. parisi* spores as L1 larvae, and reporter expression was measured at 30 hpi. (B and D) *N. parisi* pathogen load assayed (Continued on next page)

IPR activation by Orsay virus. Worms raised on *dcr-1* RNAi beginning at the L1 stage and infected with Orsay virus at L4 showed higher levels of IPR activation at 24 hpi than worms raised on the RNAi vector control and also carried a higher viral load (Fig. 3G to I), indicating that DCR-1 is not required for IPR activation by Orsay virus. Altogether, these results indicate that DRH-1, but not other canonical RNAi factors like DCR-1, is required for mediating the induction of IPR gene expression upon viral infection.

**IPR gene expression is induced in a manner dependent on DRH-1 and on the activity of Orsay virus RNA-dependent RNA polymerase.** Previous work indicated that transgenic expression and replication of only Orsay virus RNA1, the viral genome segment containing the RDRP, was sufficient to activate the *pals-5p::GFP* IPR reporter and that this activation was lost when a mutation was introduced that ablated the polymerase activity of the RDRP (and therefore also ablated the replication of the RNA1 segment) (30). Here, we investigated whether this effect was dependent on DRH-1. First, we compared IPR reporter expression in transgenic animals expressing Orsay virus wild-type RNA1 [RNA1(wt)] or Orsay virus RNA1 D601A (RDRP-defective mutant) under the control of a heat shock promoter in a *WT* or *drh-1* mutant background. We found that, in agreement with previous work, heat shock-induced expression and replication of Orsay virus RNA1(wt) in the *WT* background led to an increase in IPR reporter expression, whereas ectopic expression of the RNA1 mutant [RNA1(mt)] did not (Fig. 4A). Importantly, we found that in the *drh-1* mutant background, neither the RNA1(wt) nor the RNA1(mt) construct was able to induce IPR reporter expression, indicating that *pals-5p::GFP* induction by Orsay virus RNA1(wt) is dependent on DRH-1 (Fig. 4A). We tested the specificity of the requirement for DRH-1 in activating the IPR in response to RNA1 RDRP activity by crossing the RNA1(wt) array into the *rde-1*, *rde-4*, and *drh-3* mutant backgrounds. We found that neither *rde-1*, *rde-4*, nor *drh-3* was required to induce *pals-5p::GFP* expression in response to heat shock-induced ORV RNA1(wt) expression (Fig. 4B), confirming that IPR activation resulting from RNA1 RDRP activity occurs via a pathway distinct from the canonical antiviral RNAi pathway.

We next investigated whether other IPR genes are induced by the expression of RNA1 and whether this induction is dependent on DRH-1. We performed qRT-PCR on animals expressing RNA1(wt) and RNA1(mt) in both *WT* and *drh-1(-)* backgrounds. First, we found that ectopic expression of RNA1(wt) induced all IPR genes tested, and this induction was dependent on *drh-1* (Fig. 4C). Analysis of the Orsay virus RNA1 transcript levels showed that RNA1 accumulated to higher levels in the *drh-1* mutants than in the *WT* controls (Fig. 4D), indicating that the lack of induction was not due to a lack of this RNA1 trigger.

**The full repertoire of IPR genes can be induced by Orsay virus RNA-dependent RNA polymerase activity, dependent on DRH-1.** Given that the ectopic expression of RNA1(wt) was sufficient to induce the expression of a subset of IPR genes (Fig. 4C), we examined the full transcriptomic response to RNA1(wt) expression using RNA-seq and investigated whether responses were dependent on DRH-1. To minimize the contribution of the RNAi pathway, we used the *rde-1(ne219)* RNAi-deficient mutant background for all of our comparisons. Specifically, we compared the following strains and used heat shock to induce RNA1 expression in all strains before harvesting RNA for RNA-seq (Fig. 5A): (i) *rde-1(-); RNA1(wt)*, (ii) *rde-1(-); RNA1(mt)*, (iii) *drh-1(-); rde-1(-); RNA1(wt)*, and (iv) *drh-1(-); rde-1(-); RNA1(mt)*. For simplicity, we refer to these strains as (i) *drh-1(+)* animals expressing RNA1(wt), (ii) *drh-1(+)* animals expressing RNA1(mt), (iii) *drh-1(-)* mutants expressing RNA1(wt), and (iv) *drh-1(-)* mutants expressing RNA1(mt).

## FIG 2 Legend (Continued)

by *N. parisi*-specific FISH staining. (E and F) *pals-5p::GFP* IPR reporter expression in worms treated with 2.5  $\mu$ M bortezomib. (G and H) *pals-5p::GFP* reporter expression in worms subjected to 24 h of 28°C heat stress beginning at the L4 stage. (I) *pals-5p::GFP* reporter fluorescence in *pals-22(jy1)* single mutants, *drh-1(ok3495)* single mutants, and *pals-22(jy1); drh-1(ok3495)* double mutants. For all panels, fluorescence and length of animals were measured for ~1,000 individual worms per experimental replicate using a Copas Biosorter instrument, with each animal represented as a dot. The graph shows combined results of three independent experimental replicates, with total numbers indicated. Means were compared using one-way ANOVA with Bonferroni correction. NS, not significant; \*\*\*\*,  $P < 0.0001$ .



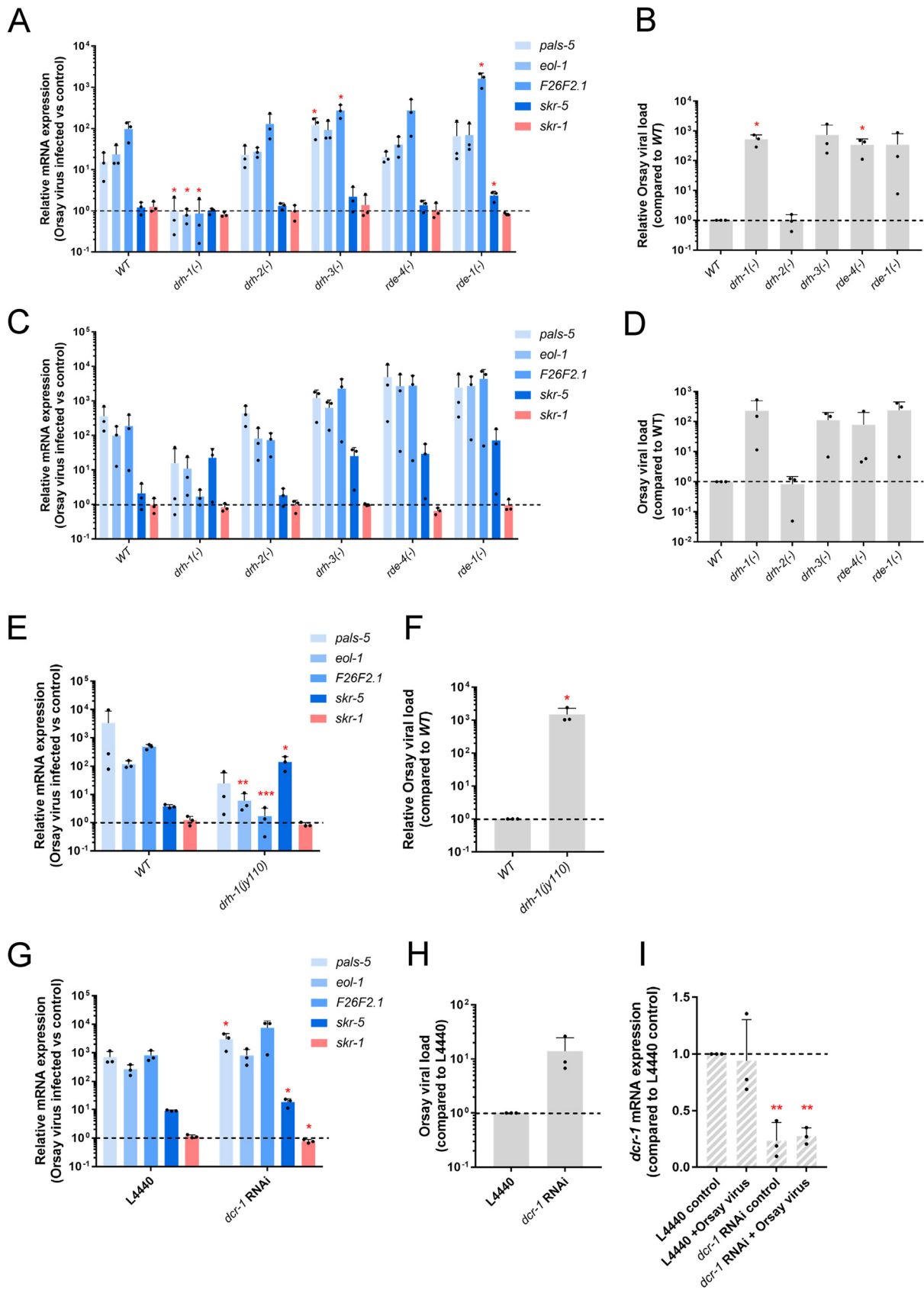


**FIG 3** DRH-1 acts independently of other RNAi factors to mediate IPR induction. (A) Induction of IPR genes analyzed by qRT-PCR in RNAi pathway mutants after 12 h of Orsay virus infection. (B) qRT-PCR assay of Orsay viral loads in RNAi pathway mutants after 12 h of Orsay virus (Continued on next page)

First, we used qRT-PCR to measure the level of RNA1 expressed in the triplicate RNA samples used for RNA-seq analysis of these four strains. Here, we saw that the levels of RNA1 were much higher in animals expressing RNA1(wt) than in those expressing RNA1(mt) (Fig. 5B), which is expected given that RNA1 is a polymerase that amplifies the copy number of RNA1. RNA1 expression levels were slightly higher on average in the *drh-1(-)* animals expressing RNA1(wt) than in *drh-1(+)* animals expressing RNA1(wt) (Fig. 5B). Next, we performed RNA-seq and used multidimensional scaling analysis on the RNA-seq results to determine which strain had the most distinct gene expression profile. Here, we found that mRNA expression in *drh-1(+)* animals expressing RNA1(wt) diverged most dramatically from mRNA expression in the other three strains (Fig. 5C), indicating a transcriptional response dependent on RDRP activity and wild-type *drh-1*.

When we compared *drh-1(+)* animals expressing RNA1(wt) to *drh-1(+)* animals expressing RNA1(mt), we found 194 genes significantly upregulated and 1 gene significantly downregulated (Fig. 6A; see also Table S1 in the supplemental material). Of these, only 26 genes were also significantly upregulated in *drh-1(-)* animals expressing RNA1(wt) versus *drh-1(-)* animals expressing RNA1(mt) (Fig. 6A and B and Table S2). These results indicate that the transcriptional response to RDRP activity is largely dependent on DRH-1. Importantly, there was also a large degree of overlap between genes induced by RDRP activity and “canonical” IPR genes, which were defined by being induced by *N. parisii* infection and regulated by *pals-22/25* (22). A majority of the IPR genes induced by RNA1(wt) were *drh-1* regulated (Fig. 6B and Table S2). For example, predicted ubiquitin ligase components, like the Cullin gene *cul-6*, which is required for increased thermotolerance in *pals-22* mutants (24), as well as the Skp-related protein gene *skr-4* and the F-box protein gene *fbxa-75*, were induced by RNA1(wt) expression in a *drh-1*-dependent manner (Table S2). We also compared the genes induced by RNA1 activity with a previously reported data set of genes induced in the *rde-1* mutant background by Orsay virus infection (21) and found that the majority of the RDRP activity-induced genes were also induced during natural Orsay virus infection (Fig. 6A to C and Table S2). While there were genes listed as being virally induced that were not significantly upregulated by the expression of RNA1(wt), most of these were induced but failed to meet the significance cutoff (Table S3). Therefore, the IPR, which is a common response to molecularly divergent pathogens like microsporidia and virus, can be induced by the expression of replication-competent Orsay virus RNA1 in a manner dependent on RDRP activity and DRH-1.

## DISCUSSION

The field of innate immunity in *C. elegans* is only about 20 years old and thus is relatively new compared to innate immunity research in other model hosts (31–34). While transcriptional responses to diverse pathogens have been described in *C. elegans*, the pattern recognition receptors that activate these responses have remained mostly unclear, with the exception of a G-protein-coupled receptor required to sense ligands induced by both wounding and fungal infection that penetrates the epidermis (32, 35). Here, we show that one of the only pattern recognition receptors conserved between mammals and *C. elegans*, DRH-1/RIG-I, appears to sense viral intermediates to trigger

### FIG 3 Legend (Continued)

infection. (C) Induction of IPR genes analyzed by qRT-PCR in RNAi pathway mutants after 24 h of Orsay virus infection. (D) qRT-PCR assay of Orsay viral loads in RNAi pathway mutants after 24 h of Orsay virus infection. (E) Induction of IPR genes by qRT-PCR in *drh-1(jy110)* mutants after 24 h of Orsay virus infection. (F) qRT-PCR assay of Orsay viral loads in *drh-1(jy110)* mutants after 24 h of Orsay virus infection. (G) Induction of IPR genes by qRT-PCR in worms treated with RNAi against *dcr-1* after 24 h of Orsay virus infection. (H) qRT-PCR assay of Orsay virus pathogen loads in worms treated with RNAi against *dcr-1* after 24 h of Orsay virus infection. (I) qRT-PCR assay of *dcr-1* transcript levels in samples from panel G. *dcr-1* levels are expressed as ratios to levels in the L4440 mock-infected control. For panels A, C, E, and G, IPR gene expression is shown as a ratio of Orsay virus-infected worms to mock-infected controls for each genotype. For panels B, D, F, and H, the Orsay viral load was assessed by Orsay virus RNA1 transcript levels compared to levels in Orsay virus-infected *WT* worms. For all panels, graphs show combined results of three independent experimental replicates, with ~1,000 animals collected for RNA in each replicate. Individual replicates are indicated by a dot, with columns representing combined means and error bars representing SD. For each transcript assessed, the mean ( $n = 3$ ) for each genotype was compared to the *WT* mean using unpaired one-tailed Student's *t* test. \*,  $P < 0.05$ ; \*\*,  $P < 0.01$ .

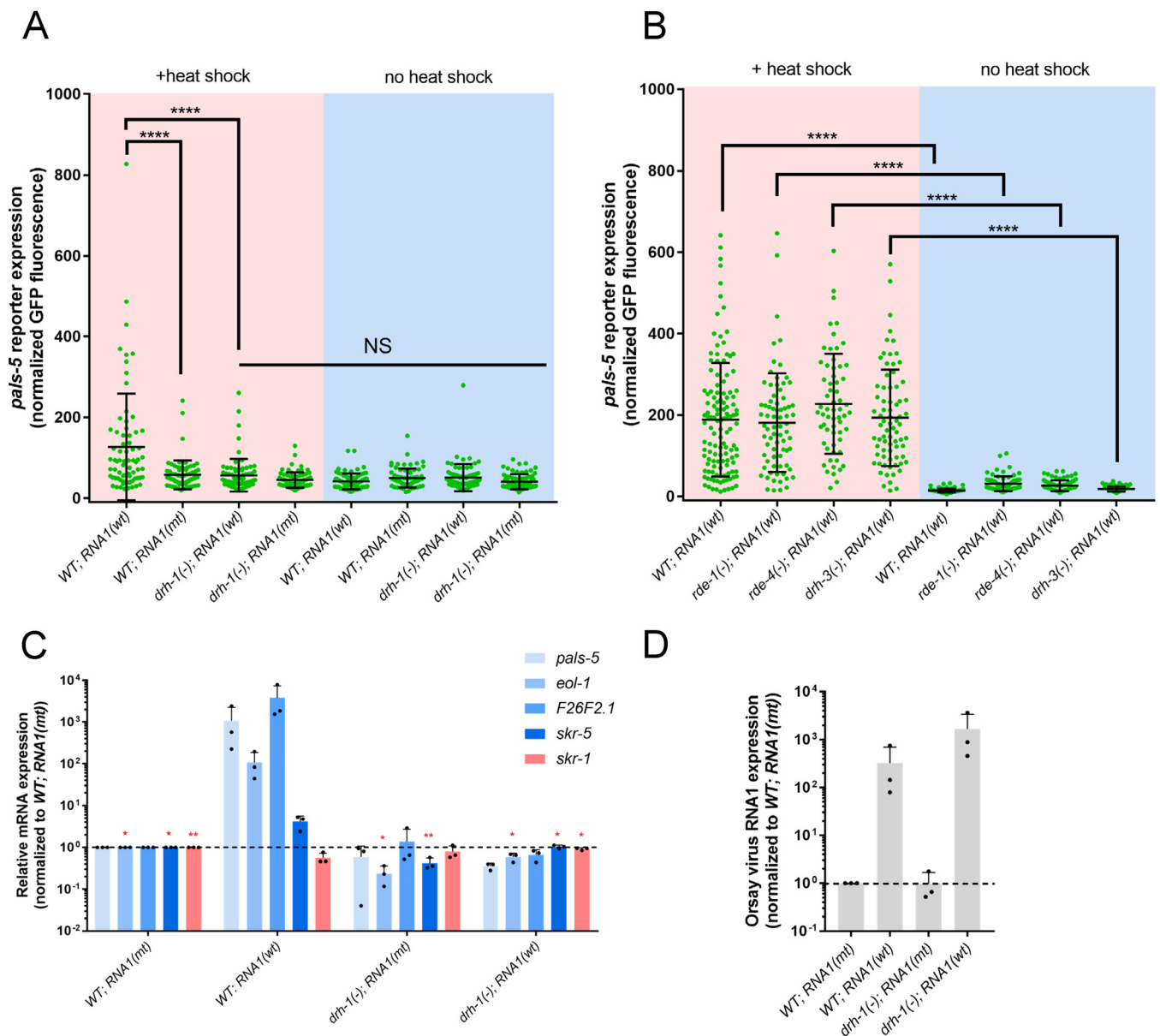


**FIG 4** RDRP activity of Orsay virus RNA1 is required for DRH-1-mediated IPR activation. (A) Quantification of *pals-5p::GFP* reporter fluorescence after heat shock induction of RNA1(wt) or RNA1(mt) expression in *WT* and *drh-1(ok3495)* backgrounds. The graph shows combined results of 3 independent experimental replicates ( $n \geq 70$ ). Means were compared using one-way ANOVA with Bonferroni correction. NS, not significant; \*\*\*\*,  $P < 0.0001$ . (B) Quantification of *pals-5p::GFP* reporter fluorescence after heat shock induction of RNA1(wt) expression in *WT*, *rde-1(ne219)*, *rde-4(ne301)*, and *drh-3(ne4253)* backgrounds. The graph shows combined results of 3 independent biological replicates for each mutant genotype ( $n \geq 60$ ) and 5 replicates for *WT* worms ( $n = 125$ ). Means were compared using one-way ANOVA with Bonferroni correction. \*\*\*\*,  $P < 0.0001$ . (C) qRT-PCR analysis of IPR gene expression after heat shock induction of RNA1(wt) versus RNA1(mt) in the *WT* and *drh-1(ok3495)* backgrounds. IPR gene expression is normalized to the expression in *WT; RNA1(mt)* animals. The graph shows combined results of 3 independent experimental replicates, and error bars represent SD. For each transcript assessed, the mean ( $n = 3$ ) for each genotype was compared to the *WT; RNA1(wt)* mean using unpaired one-tailed Student's *t* test. \*,  $P < 0.05$ ; \*\*,  $P < 0.01$ . (D) qRT-PCR analysis of RNA1 transcript levels after heat shock induction of RNA1(wt) and RNA1(mt) in *WT* and *drh-1(ok3495)* backgrounds. RNA1 transcript levels are compared to RNA1 levels in *WT; RNA1(mt)* animals. The graph shows combined results of 3 independent experimental replicates, and error bars represent SD. The mean ( $n = 3$ ) for each genotype was compared to the *WT; RNA1(mt)* mean using unpaired one-tailed Student's *t* test. No significant differences were found.

the IPR transcriptional program in the intestine, which is associated with increased defense against Orsay virus and other intracellular pathogens (22). Importantly, the role of *drh-1* in mediating the *C. elegans* transcriptional response to Orsay virus is separable from its role in antiviral RNAi, as neither of the two known direct binding partners of DRH-1, RDE-4 and DCR-1, nor other RNAi pathway components that we tested were required for IPR activation. Because the RDRP activity from the Orsay virus RNA1

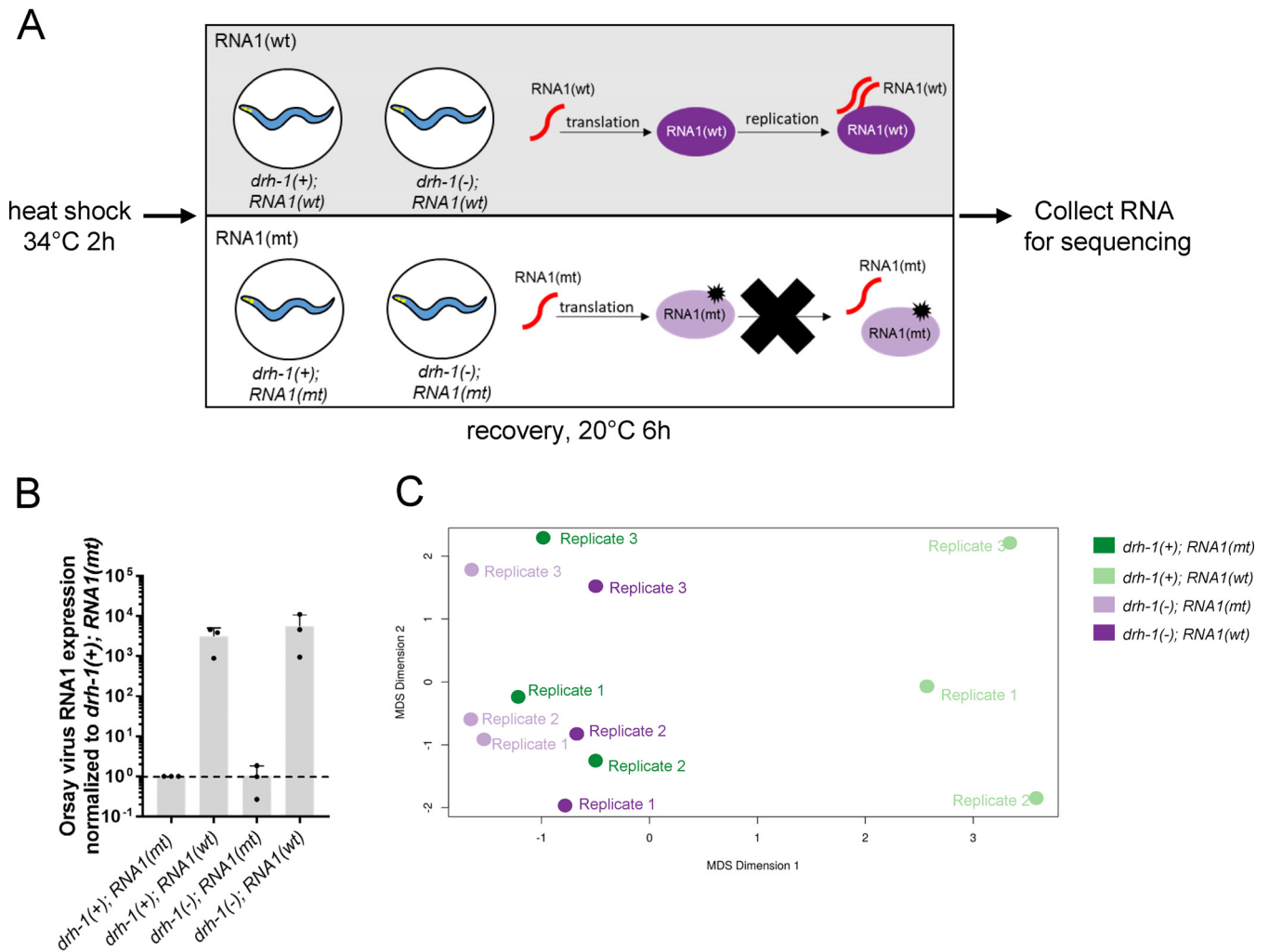


**FIG 5** Characterization of the transcriptional response to Orsay virus RNA1. (A) Schematic of sample preparation for RNA-seq. Synchronized populations of L1 larvae of all four genotypes [*drh-1(+); RNA1(mt)*, *drh-1(+); RNA1(wt)*, *drh-1(-); RNA1(mt)*, and *drh-1(-); RNA1(wt)*] were obtained by Copas Biosorter-based isolation of animals with the transgenic array marker *myo-2p::YFP* to obtain a relatively pure population of transgene-positive animals. After sorting, worms were plated with food and incubated at 20°C for 2 days until the L4 stage. At the L4 stage, worms were subjected to a 2-h heat shock at 34°C to induce the expression of RNA1. Worms were recovered at 20°C for 6 h and then harvested for RNA isolation. (B) qRT-PCR analysis of RNA1 transcript levels in samples used for RNA-seq. RNA1 transcript levels are normalized to RNA1 levels in *drh-1(+); RNA1(mt)* worms. The graph shows combined results for all three RNA-seq replicates; bars represent means, and error bars represent SD. The mean ( $n = 3$ ) for each genotype was compared to the *WT*; *RNA1(mt)* mean using unpaired one-tailed Student's  $t$  test. No significant differences were found. (C) Multidimensional scaling (MDS) plot of all three RNA-seq replicates.

segment appears to be required for activation, our results suggest that a viral replication intermediate, such as dsRNA or 5'-triphosphorylated RNA, is the ligand that binds the DRH-1 receptor to activate the IPR (Fig. 4 to 6). This pathogen ligand-pattern recognition receptor pair is one of the few that have been paired together so far in *C. elegans*. Of note, we found that microsporidian induction of the IPR is independent of DRH-1, indicating that there are separate receptors yet to be identified that sense infection with these fungus-related pathogens. It is possible that microsporidia are sensed by the proteotoxic stress that they cause during infection, although given the large number of effectors secreted by microsporidia (36), there are likely receptors that sense specific microsporidian ligands to trigger the IPR.

What happens downstream of DRH-1 activation to induce IPR gene expression? *C. elegans* does not have clear homologs of MAVS, IRF3, and NF- $\kappa$ B, which activate the transcriptional program downstream of RIG-I-like receptors in mammals (5). Therefore, the signaling components that mediate this response in *C. elegans* are likely to be different. So far, the only other host factors shown to regulate the activation of the IPR

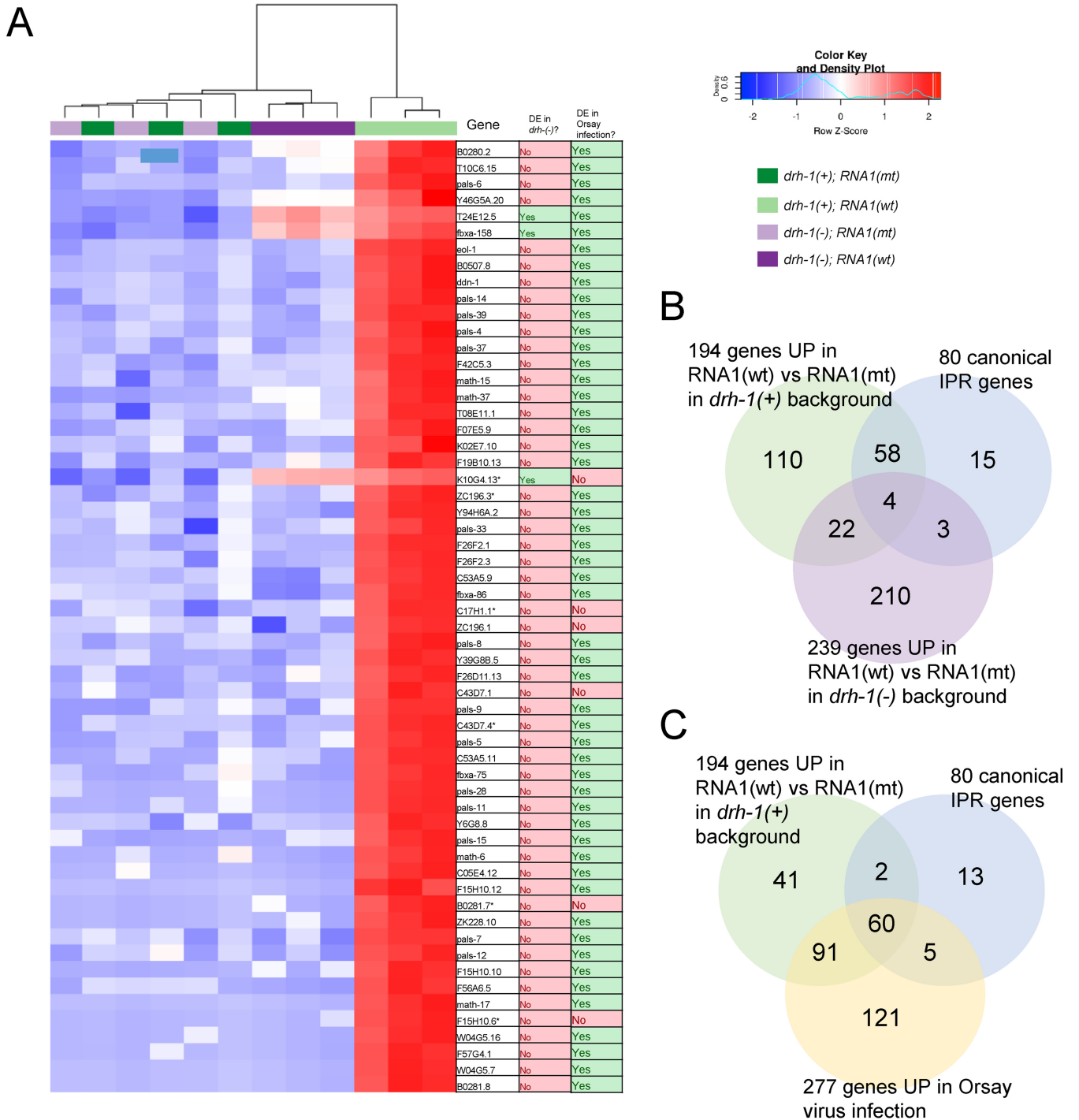


**FIG 6** Ectopic expression of Orsay virus RNA1 induces the IPR gene repertoire in an RDRP-dependent and DRH-1-dependent manner. (A) Heat map showing the top ( $P < 0.003$ ) differentially expressed (DE) genes in *drh-1(+); RNA1(wt)* versus *drh-1(+); RNA1(mt)* worms. \* denotes pseudogenes. Columns indicate whether the gene was also differentially expressed in *drh-1(-); RNA1(wt)* versus *drh-1(-); RNA1(mt)* worms and whether the gene was also differentially expressed in the Orsay virus-infected *rde-1* mutant data set (21). (B) Overlap between genes significantly upregulated by RNA1(wt) in the *drh-1(+)* background with canonical IPR genes and between genes significantly upregulated by RNA1(wt) in the *drh-1(-)* background. (C) Overlap between genes significantly upregulated by RNA1(wt) in the *drh-1(+)* background with canonical IPR genes and between genes significantly upregulated by Orsay virus infection as described previously by Chen et al. (21).

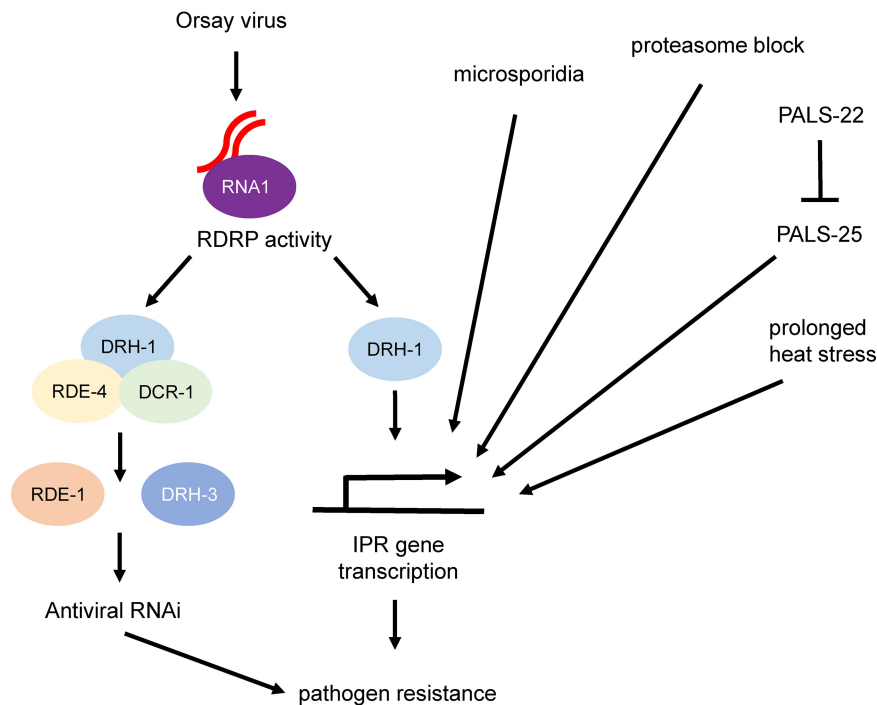


**FIG 7** Model of DRH-1-mediated IPR activation by Orsay virus. Orsay virus infection in *C. elegans* is detected by DRH-1 recognition of viral replication intermediates produced by Orsay virus RNA-dependent RNA polymerase activity. DRH-1 signals downstream to activate the transcription of the protective IPR. In parallel, DRH-1 also participates in the production of antiviral RNAi. The IPR can also be triggered by microsporidian infection, prolonged heat stress, proteasome blockade, and mutations in *pals-22*. Unlike viral infection, these triggers do not require DRH-1.

are the antagonistic paralogs PALS-22 and PALS-25, which repress and activate the IPR, respectively (22). DRH-1 appears to act in parallel to both PALS-22 and external triggers of the IPR, like microsporidian infection and proteotoxic stress. These findings indicate that DRH-1 is just one of multiple inputs to the IPR (Fig. 7). While constitutive activation of IPR gene expression in PALS-22 mutants indicates that this transcriptional program provides antiviral defense (22), the contribution of DRH-1-mediated induction of this program is less clear. In previous studies, it appeared that DRH-1 might have a role independent of RNAi in antiviral defense, as the loss of both DRH-1 and RNAi factors together led to greater susceptibility to infection than the loss of the RNAi factors alone (12). We also observed a trend toward higher levels of accumulation of Orsay virus RNA1 transcripts in the *rde-1(-); drh-1(-)* double mutant background than in the *rde-1(-)* single mutant background (Fig. 5B), which would be consistent with this model. Indeed, *drh-1* does not appear to be required for antiviral siRNA biogenesis but rather appears to regulate which regions of the viral RNA are converted into small interfering RNAs (13). It is not currently possible to completely separate the effects of DRH-1 activity on RNAi from its effects on IPR activation, but it is possible that some of the viral susceptibility in *drh-1* mutants that has been attributed to defects in antiviral RNAi could instead be due to defects in IPR activation.

In mammals, a prominent output of RIG-I signaling is transcriptional upregulation of interferon genes that encode ligands to activate interferon receptors and downstream signaling. Because *C. elegans* lacks interferon orthologs, it will be interesting to determine the nature of IPR effectors and how they regulate resistance. Of note, *C. elegans* has homologs of the STAT transcription factors, which act downstream of the interferon receptor in mammals to activate interferon-stimulated genes and promote antiviral defense (37–39). Surprisingly, the *sta-1* STAT transcription factor appears to repress the expression of viral response genes, and *sta-1* mutants are resistant to infection (19). This result highlights another difference between mammals and *C. elegans* in terms of the

**TABLE 1** *C. elegans* strains used in this study

Strain	Genotype
ERT054	<i>jyls8[pals-5p::GFP; myo-2p::mCherry] X</i>
ERT712	<i>drh-1(ok3495) IV; jyls8[pals-5p::GFP; myo-2p::mCherry] X</i>
ERT286	<i>pals-22(jy1) III; jyls8[pals-5p::GFP; myo-2p::mCherry] X</i>
ERT782	<i>pals-22(jy1) III; drh-1(ok3495) IV; jyls8[pals-5p::GFP; myo-2p::mCherry] X</i>
N2	N2
WM27	<i>rde-1(ne219) V</i>
WM49	<i>rde-4(ne301) III</i>
RB2519	<i>drh-1(ok3495) IV</i>
RB1024	<i>drh-2(ok951) IV</i>
WM206	<i>drh-3(ne4253) I</i>
ERT767	<i>virEx23[HSP::OrsayRNA1; myo-2p::YFP]</i>
ERT768	<i>virEx26[HSP::OrsayRNA1 D601A; myo-2p::YFP]</i>
ERT695	<i>jyls8[pals-5p::GFP; myo-2p::mCherry] X; virEx23[HSP::OrsayRNA1; Pmyo-2::YFP]</i>
ERT697	<i>jyls8[pals-5p::GFP; myo-2p::mCherry] X; virEx26[HSP::OrsayRNA1 D601A; Pmyo-2::YFP]</i>
ERT696	<i>drh-1(ok3495) IV; jyls8[pals-5p::GFP; myo-2p::mCherry] X; virEx23[HSP::OrsayRNA1; myo-2p::YFP]</i>
ERT698	<i>drh-1(ok3495) IV; jyls8[pals-5p::GFP; myo-2p::mCherry] X; virEx26[HSP::OrsayRNA1 D601A; myo-2p::YFP]</i>
WUM51	<i>rde-1(ne219) V; jyls8[pals-5p::GFP; myo-2p::mCherry] X; virEx23[HSP::OrsayRNA1; myo-2p::YFP]</i>
ERT808	<i>rde-4(ne301) III; jyls8[pals-5p::GFP; myo-2p::mCherry] X; virEx23[HSP::OrsayRNA1; myo-2p::YFP]</i>
ERT802	<i>drh-3(ne4253) I; jyls8[pals-5p::GFP; myo-2p::mCherry] X; virEx23[HSP::OrsayRNA1; myo-2p::YFP]</i>
ERT765	<i>drh-1(ok3495) IV; virEx23[HSP::OrsayRNA1; myo-2p::YFP]</i>
ERT766	<i>drh-1(ok3495) IV; virEx26[HSP::OrsayRNA1 D601A; myo-2p::YFP]</i>
ERT805	<i>rde-1(ne219) V; virEx23[HSP::OrsayRNA1; myo-2p::YFP]</i>
ERT806	<i>rde-1(ne219) V; virEx26[HSP::OrsayRNA1 D601A; myo-2p::YFP]</i>
ERT803	<i>drh-1(ok3495) IV; rde-1(ne219) V; virEx23[HSP::OrsayRNA1; myo-2p::YFP]</i>
ERT804	<i>drh-1(ok3495) IV; rde-1(ne219) V; virEx26[HSP::OrsayRNA1 D601A; myo-2p::YFP]</i>
ERT780	<i>drh-1(jy110) IV; jyls8[pals-5p::GFP; myo-2p::mCherry] X</i>
ERT709	<i>drh-1(jy110) IV</i>

signaling events downstream of RIG-I recognition of viral infection. While a RIG-I ortholog has not been reported in insects, an antiviral role for Dicer2 (which is a DExD/H box helicase like RIG-I) has been shown in *Drosophila* and mosquitoes, where it is required for NF- $\kappa$ B-induced transcription of an interferon analog (40, 41). Thus, there may be related but distinct mechanisms of transcriptional induction directed by DExD/H box helicases upon viral infection in mammals, insects, and *C. elegans*.

One intriguing theme in common between RIG-I/IPR signaling in *C. elegans* and the RIG-I/interferon response in mammals is that defects in the proteasome are associated with both responses. Previous work in *C. elegans* demonstrated that either a genetic or pharmacological block of the proteasome will activate IPR gene expression, in a manner independent of canonical proteostasis factors like the SKN-1/Nrf2 transcription factor (20, 22). In humans, mutations in the proteasome, as well as gain-of-function mutations in RIG-I-like receptors, can lead to inappropriate activation of type I interferon responses and autoimmunity (42). These defects are part of a group of diseases called interferonopathies, which are associated with upregulation of interferon, although it is controversial whether interferon is causal for these diseases (43, 44). Therefore, it is possible that mammalian RIG-I triggers an interferon-independent output similar to the IPR that promotes both immunity and damaging inflammation. In light of this idea, it is interesting to note that constitutive activation of the IPR in *pals-22* mutants is associated with increased immunity but also fitness defects such as shortened life span and premature aging (24). Therefore, further analysis of the regulation and outputs of the IPR may shed light on the interplay between viral infection, immunity, and the negative consequences of hyperactivation of immune responses.

## MATERIALS AND METHODS

***C. elegans* strains and maintenance.** *C. elegans* were maintained on nematode growth medium (NGM) plates seeded with OP50 *Escherichia coli* as previously described (45). Worms were maintained at 20°C unless otherwise noted. See Table 1 for a list of all *C. elegans* strains used in this study.

**CRISPR deletion of the *drh-1* locus.** To generate a mutant with a deletion of the entire *drh-1* genomic locus, we used the CRISPR coconversion strategy (46). The following two CRISPR RNAs (crRNAs) targeting either side of the *drh-1* genomic locus were designed using Chopchop (<https://chopchop.cbu.uib.no/>): GCGTCTCTACTAATACAC and GGTTTTGGTCATCTTGATGT. *drh-1* crRNAs, *dpy-10* crRNA, and

*trans*-acting crRNA (tracrRNA) were obtained from IDT and resuspended in IDT nuclease-free duplex buffer. CRISPR injection mix was constructed and contained 0.5  $\mu$ l 100  $\mu$ M *dpy-10* crRNA, 0.5  $\mu$ l 100  $\mu$ M *drh-1* crRNAs, 2.5  $\mu$ l 100  $\mu$ M tracrRNA, and 3.5  $\mu$ l Cas9 (QB3 MacroLab). The Cas9 mixture was then injected into the gonad of approximately 30 young adult N2 worms. Injected worms were transferred singly onto individual NGM OP50 plates and incubated at 20°C for 3 to 4 days. Plates with a large number of F1 progeny showing the Dpy phenotype were identified, and >100 individual Dpy<sup>+</sup> F1 progeny were picked onto individual plates. Once F1 progeny had laid eggs, they were lysed and genotyped for the deletion of the *drh-1* locus using primers deletion external forward (CTCGTACCAGTGCAGAAATA) and deletion internal reverse (CCAACCGCAATTCCAACATC). The presence of the complete deletion was confirmed with Sanger sequencing, and the allele was designated *drh-1(jy110)*. The *dpy-10* mutation was crossed out of the *drh-1(jy110)* background, and *drh-1(jy110)* mutants were backcrossed three times to N2 prior to use in experiments.

**Orsay virus filtrate preparation.** Orsay virus filtrates were prepared as previously described (17). Briefly, infected *rde-1(ne219)* worms were grown on standard NGM OP50 plates until just starved, washed off plates using M9 buffer, and disrupted with silicon beads. The homogenate was then filtered through a 0.22- $\mu$ m filter, and aliquots were flash frozen in liquid nitrogen.

**Orsay virus infection.** For L1 infection (Fig. 1A), adults were bleached to obtain synchronized L1 larvae, which were then mixed with a 10 $\times$  concentration of OP50 *E. coli* and a 1:50 dilution of the Orsay virus filtrate. Next, a 500- $\mu$ l total volume of an L1-food-virus mix was plated onto 6-cm unseeded NGM plates and dried in a laminar flow hood. Infected worms were then incubated at 20°C until collection.

For L2 infection (Fig. 1B to F), bleached L1 larvae were plated onto 6-cm NGM plates containing a lawn of OP50 *E. coli* and incubated at 20°C overnight prior to infection. The Orsay virus filtrate was then diluted in M9 buffer at a ratio of 1:50. Three hundred microliters of a 1:50 dilution of the filtrate was top plated onto the plates, which were then dried in a laminar flow hood. Infected worms were incubated at 20°C for 24 h prior to collection.

For L4 infection (Fig. 3), 10  $\mu$ l of the Orsay virus filtrate was mixed with 300  $\mu$ l of a 10 $\times$  concentration of OP50 *E. coli* and 190  $\mu$ l M9 buffer, and 500  $\mu$ l of this mixture was seeded onto 6-cm NGM plates and dried in a laminar flow hood. L4-stage worms (bleached L1 larvae plated onto standard 6-cm OP50 plates and incubated at 20°C for 2 days) were washed off plates using M9 buffer plus 0.1% Triton X-100 (TX-100), counted, and replated onto plates seeded with the Orsay virus filtrate mix. Infected worms were incubated at 20°C for the indicated amounts of time prior to collection.

***pals-5p::GFP* quantification. (i) *pals-5p::GFP* quantification by using a worm sorter.** Worms were washed off plates into microcentrifuge tubes using M9 buffer plus 0.1% TX-100 and then washed three times with M9 buffer plus 0.1% TX-100. Worms were concentrated into 150 to 200  $\mu$ l and transferred into 96-well cell culture plates. Worms were then analyzed using a Copas Biosort instrument (Union Biometrica) to record the time of flight (TOF) and green fluorescence for each worm. The GFP signal (in arbitrary fluorescence units) was normalized to worm size by dividing fluorescence by TOF for each worm (Fig. 1B and E and Fig. 2).

**(ii) *pals-5p::GFP* quantification by using ImageJ.** Worms were collected and washed as described above and then paralyzed by adding 2  $\mu$ l 5 M sodium azide. Worms were then mounted onto 2% agarose pads on glass slides, sealed with a coverslip, and imaged using a Zeiss AxioImager M1 upright fluorescence microscope with a 10 $\times$  objective. The signal was collected for differential interference contrast (DIC), yellow fluorescent protein (YFP) (coinjection marker for the heat shock Orsay virus RNA1 expression array), GFP (*pals-5p::GFP*), and mCherry (*pals-5p::GFP* coinjection marker). Identical exposure times were used for all images within an experiment. The GFP signal in the intestine of individual worms was quantified using ImageJ (<https://imagej.nih.gov/ij/>). Mean gray values for each intestine were normalized by subtracting the mean gray value from the image background (Fig. 3A and B).

***N. parisii* infection.** The *N. parisii* ERTm1 spore filtrate was prepared as previously described (47). A total of 1,200 bleached L1 larvae were combined with 500,000 ERTm1 spores, 150  $\mu$ l of a 10 $\times$  concentration of OP50 *E. coli*, and M9 buffer to a total volume of 300  $\mu$ l; seeded onto 6-cm NGM plates; and dried in a laminar flow hood. ERTm1-infected worms were incubated at 25°C for 30 h prior to collection.

***N. parisii* pathogen load.** *N. parisii* pathogen load was assessed by fluorescence *in situ* hybridization (FISH) staining as previously described (22). Briefly, infected worms were fixed in 4% paraformaldehyde and then hybridized with a CalFluor610-tagged FISH probe (Biosearch) specific for *N. parisii* rRNA. FISH-stained worms were analyzed using a Copas Biosort instrument (Union Biometrica) to record TOF and red fluorescence for each individual worm. The signal was normalized to the worm size by dividing red fluorescence (in arbitrary fluorescence units) over the TOF for each worm.

**Bortezomib treatment.** Bleached L1 larvae were plated onto 6-cm NGM plates containing a lawn of OP50 *E. coli* and incubated at 20°C overnight. A 10  $\mu$ M stock solution of bortezomib (Selleck Chemicals) resuspended in dimethyl sulfoxide (DMSO) was mixed with M9 buffer and top plated onto plates for a final concentration of 2.5  $\mu$ M bortezomib per plate. Control plates were top plated with an equal amount of DMSO in M9 buffer. Plates were then incubated at 20°C for 24 h prior to analysis with the Copas Biosort instrument (Union Biometrica).

**Prolonged heat stress.** Bleached L1 larvae were plated onto 6-cm NGM plates containing a lawn of OP50 *E. coli* and incubated at 20°C overnight. Experimental plates were then incubated at 28°C for 24 h, while control plates remained at 20°C. Worms were analyzed after 24 h using the Copas Biosort instrument (Union Biometrica).

**qRT-PCR.** Approximately 1,000 worms per sample were washed off plates, washed with M9 buffer, and then concentrated into <50  $\mu$ l. Worms were homogenized in TRI reagent (Molecular Research



**TABLE 2** qRT-PCR primers used in this study

Gene	Primer	Primer sequence
<i>snb-1</i>	snb-F1	CCGGATAAGACCATCTTGACG
	snb-R1	GACGACTTCATCAACCTGAGC
<i>pals-5</i>	C17H1.6_F1	CATTGGAAAGCGATATTGGA
	C17H1.6_R1	TCTCCAGGCACCTATCTTGTAG
<i>eol-1</i>	eol-1 qPCR FWD	GAAGGAGGTGGCGATGTTTAT
	eol-1 qPCR REV	CGGCGTCGATTGTCTCTTT
<i>F26F2.1</i>	F26F2.1_F1	TGGAACCAAGTTCAGAGACAC
	F26F2.1_R1	TTGTGAGAATTTCCGCGATA
<i>skr-5</i>	skr-5_F1	CGAAGAGCAAGATGTCAAATTTG
	skr-5_R1	AGAAGCTTGGATTGATTGGCA
<i>skr-1</i>	skr-1_F1	GGCAAAGGAACGCGAAATCA
	skr-1_R1	TTGAGAGACGGATCACATTGC
<i>dcr-1</i>	dcr-1 qPCR F1	GCTAGTGATTTAGTCTCGCTCTC
	dcr-1 qPCR R1	TACCCAGGCACCCAATTTTC
<i>yfp</i>	YFP qPCR_F1	TCGCCAGATACCCAGATCATA
	YFP qPCR_R1	GTGTCTTGTAGTCCCGTCATC
<i>OrsayRNA1</i>	GW194	ACCTCACAAGTCCATCTACA
	GW195	GACGCTTCCAAGATTGGTATTGGT

Center, Inc.) and frozen at  $-80^{\circ}\text{C}$ . RNA was extracted using TRI reagent and 1-bromo-3-chloropropane (BCP) (Molecular Research Center, Inc.) according to the manufacturer's instructions. cDNA was prepared from total RNA using either SuperScript Vilo (Thermo Fisher) or iScript (Bio-Rad) cDNA synthesis kits. qRT-PCR was performed using iQ SYBR green supermix (Bio-Rad) on a CFX connect real-time system. Each experimental replicate was measured in technical duplicate. All gene expression was normalized to *snb-1* expression, which does not change upon conditions tested. For comparisons of strains containing the *Ex[HSP::RNA1]* arrays, gene expression was additionally normalized to *yfp* expression to control for array mosaicism and differing numbers of array-containing animals in the test populations. The Pfaffl method was used for quantifying gene expression changes (48). For a list of qRT-PCR primers, see Table 2.

***dcr-1* RNAi treatment.** Cultures of the Ahinger library *dcr-1 E. coli* RNAi clone or the RNAi vector control L4440 *E. coli* clone in the HT115 bacterial strain grown overnight were seeded onto 6-cm NGM plates supplemented with 5 mM isopropyl- $\beta$ -D-thiogalactopyranoside (IPTG) and 1 mM carbenicillin and incubated at room temperature for 1 day. Synchronized L1 larvae obtained by bleaching were plated onto RNAi *E. coli* lawns and grown for 48 h at  $20^{\circ}\text{C}$ . A total of 300  $\mu\text{l}$  of a 1:50 dilution of the Orsay virus filtrate was top plated onto the plates, and plates were dried in a laminar flow hood. Infected worms were incubated at  $20^{\circ}\text{C}$  for 24 h prior to collection.

**Heat shock promoter (HSP)::RNA1 heat shock induction.** Transgenic array-positive worms were picked onto standard NGM OP50 plates and allowed to reproduce for 5 days at  $20^{\circ}\text{C}$  before bleaching plates. Bleached L1 larvae were plated onto 6-cm NGM plates containing a lawn of OP50 *E. coli* and incubated at  $20^{\circ}\text{C}$  for 2 days (until the L4 stage). At the L4 stage, plates were heat shocked at  $34^{\circ}\text{C}$  for 2 h and then allowed to recover at  $20^{\circ}\text{C}$  for 6 h prior to collection.

**RNA-seq sample preparation and sequencing.** Bleached L1 larvae were sorted using a Copas Biosort instrument (Union Biometrica) to obtain a population enriched for the *Ex[HSP::RNA1(wt)]* or *Ex[HSP::RNA1(mt)]* extrachromosomal array. Array-positive larvae were sorted onto unseeded 10-cm NGM worm plates at a density of  $\sim 2,000$  worms/plate, and 1 ml of a  $10\times$  concentration of OP50 *E. coli* was added after sorting was complete. Plates were incubated at  $20^{\circ}\text{C}$  for 48 h, until the L4 stage. At the L4 stage, plates were heat shocked at  $34^{\circ}\text{C}$  for 2 h and then allowed to recover at  $20^{\circ}\text{C}$  for 6 h prior to collection. Worms were washed off plates, washed three times with M9 buffer, and then concentrated into  $<50 \mu\text{l}$ . Worms were then homogenized in 1 ml TRI reagent (Molecular Research Center, Inc.) and frozen at  $-80^{\circ}\text{C}$ . RNA was extracted using TRI reagent and BCP (Molecular Research Center, Inc.) according to the manufacturer's instructions and additionally purified using the RNeasy cleanup kit with on-column DNase I digestion (Qiagen). RNA quality was assessed by using a TapeStation system. Sequencing libraries were constructed using the TruSeq stranded mRNA method (Illumina) and sequenced using run type SR75 on an Illumina HiSeq4000 sequencer (Illumina). RNA quality assessment and RNA-seq were conducted at the IGM Genomics Center, University of California, San Diego, La Jolla, CA.

**RNA-seq analysis.** RNA-seq analysis was performed by the Center for Computational Biology and Bioinformatics at the University of California, San Diego. Quality control of the raw fastq files was performed using the software tool FastQC (49) v0.11.3. Sequencing reads were trimmed with

Trimmomatic (50) v0.36 and aligned to the *C. elegans* WBcel235 genome (51) using STAR aligner (52) v2.5.3a. Read quantification was performed with RSEM (53) v1.3.0 and the WBcel235 v96 annotation (54). The R BioConductor packages edgeR (55) and limma (56) were used to implement the limma-voom method (57) for differential expression analysis. In brief, lowly expressed genes—those not having  $\geq 1$  cpm in at least 1 of the samples—were filtered out, and trimmed mean of M values (TMM) (58) normalization was then applied. The experimental design was modeled upon genotype and treatment ( $\sim 0 + \text{genotype} + \text{treatment}$ ). The voom method was employed to model the mean-variance relationship in the log counts per minute values, after which lmFit was used to fit per-gene linear models and empirical Bayes moderation was applied with the eBayes function. Significance was defined by using an adjusted *P* value cutoff of 0.05 after multiple-testing correction (59) using a moderated *t* statistic in limma. For gene lists, WormBase version WS270 was used to remove dead genes and update gene names.

A table of normalized gene counts for all RNA-seq replicates in this study can be found in Table S4 in the supplemental material.

**Statistics. (i) Statistical analysis of Copas Biosorter fluorescence data and ImageJ fluorescence quantification.** Normalized fluorescence data from three independent experimental replicates were combined and analyzed using one-way analysis of variance (ANOVA) with Bonferroni correction to compare the mean of each group to those of every other group.

**(ii) Statistical analysis of qRT-PCR data.** For each experiment, mean expression levels were calculated from 3 independent experimental replicates. For IPR gene expression where expression levels for each genotype were normalized to values for uninfected controls of the same genotype, means were compared to *WT* values using unpaired one-tailed Student's *t* test. For viral RNA1 loads where experimental groups were normalized to infected *WT* or *RNA1(mt)* controls, means were compared to a value of 1 (no change) using unpaired one-tailed Student's *t* test.

All statistics were performed using Prism 7.

**Data availability.** All RNA-seq read files are available from the NCBI GEO database (accession number [GSE138268](https://www.ncbi.nlm.nih.gov/geo/query/acc.cgi?acc=GSE138268)).

## SUPPLEMENTAL MATERIAL

Supplemental material is available online only.

**SUPPLEMENTAL FILE 1**, XLSX file, 6.9 MB.

**SUPPLEMENTAL FILE 2**, XLSX file, 0.1 MB.

**SUPPLEMENTAL FILE 3**, XLSX file, 0.02 MB.

**SUPPLEMENTAL FILE 4**, XLSX file, 2.9 MB.

## ACKNOWLEDGMENTS

We thank R. Underwood, A. Birmingham, and K. Fisch for assistance with RNA-seq data analysis and V. Lazetic, S. Gang, I. Sfarctic, and T. Bui for suggestions on the manuscript. RNA-seq was conducted at the IGM Genomics Center, University of California, San Diego, La Jolla, CA.

This work was supported by the NIH under awards R01 AG052622 and GM114139 to E.R.T. and R21 AI133291 to D.W. J.N.S. and E.T. were supported by NIGMS/NIH award K12GM068524. The project described was partially supported by National Institutes of Health grant UL1TR001442 of the CTSA program. The content is solely the responsibility of the authors and does not necessarily represent the official views of the NIH. Some strains were provided by the CGC, which is funded by NIH Office of Research Infrastructure Programs (P40 OD010440).

## REFERENCES

- Ahmad S, Hur S. 2015. Helicases in antiviral immunity: dual properties as sensors and effectors. *Trends Biochem Sci* 40:576–585. <https://doi.org/10.1016/j.tibs.2015.08.001>.
- Lässig C, Hopfner K-P. 2017. Discrimination of cytosolic self and non-self RNA by RIG-I-like receptors. *J Biol Chem* 292:9000–9009. <https://doi.org/10.1074/jbc.R117.788398>.
- Yoneyama M, Kikuchi M, Matsumoto K, Imaizumi T, Miyagishi M, Taira K, Foy E, Loo Y-M, Gale M, Akira S, Yonehara S, Kato A, Fujita T. 2005. Shared and unique functions of the DExD/H-box helicases RIG-I, MDA5, and LGP2 in antiviral innate immunity. *J Immunol* 175:2851–2858. <https://doi.org/10.4049/jimmunol.175.5.2851>.
- Wu B, Hur S. 2015. How RIG-I like receptors activate MAVS. *Curr Opin Virol* 12:91–98. <https://doi.org/10.1016/j.coviro.2015.04.004>.
- Gebhardt A, Laudenbach BT, Pichlmair A. 2017. Discrimination of self and non-self ribonucleic acids. *J Interferon Cytokine Res* 37:184–197. <https://doi.org/10.1089/jir.2016.0092>.
- Cohen LB, Troemel ER. 2015. Microbial pathogenesis and host defense in the nematode *C. elegans*. *Curr Opin Microbiol* 23:94–101. <https://doi.org/10.1016/j.mib.2014.11.009>.
- Irazoqui JE, Urbach JM, Ausubel FM. 2010. Evolution of host innate defence: insights from *Caenorhabditis elegans* and primitive invertebrates. *Nat Rev Immunol* 10:47–58. <https://doi.org/10.1038/nri2689>.
- Pujol N, Link EM, Liu LX, Kurz CL, Alloing G, Tan MW, Ray KP, Solari R, Johnson CD, Ewbank JJ. 2001. A reverse genetic analysis of components of the Toll signaling pathway in *Caenorhabditis elegans*. *Curr Biol* 11: 809–821. [https://doi.org/10.1016/S0960-9822\(01\)00241-X](https://doi.org/10.1016/S0960-9822(01)00241-X).
- Pukkila-Worley R. 2016. Surveillance immunity: an emerging paradigm of innate defense activation in *Caenorhabditis elegans*. *PLoS Pathog* 12: e1005795. <https://doi.org/10.1371/journal.ppat.1005795>.

10. Duchaine TF, Wohlschlegel JA, Kennedy S, Bei Y, Conte D, Pang K, Brownell DR, Harding S, Mitani S, Ruvkun G, Yates JR, Mello CC. 2006. Functional proteomics reveals the biochemical niche of *C. elegans* DCR-1 in multiple small-RNA-mediated pathways. *Cell* 124:343–354. <https://doi.org/10.1016/j.cell.2005.11.036>.
11. Tabara H, Yigit E, Siomi H, Mello CC. 2002. The dsRNA binding protein RDE-4 interacts with RDE-1, DCR-1, and a DExH-box helicase to direct RNAi in *C. elegans*. *Cell* 109:861–871. [https://doi.org/10.1016/s0092-8674\(02\)00793-6](https://doi.org/10.1016/s0092-8674(02)00793-6).
12. Ashe A, BÉlicard T, Le Pen J, Sarkies P, Frézal L, Lehrbach NJ, Félix M-A, Miska EA. 2013. A deletion polymorphism in the *Caenorhabditis elegans* RIG-I homolog disables viral RNA dicing and antiviral immunity. *Elife* 2:e00994. <https://doi.org/10.7554/eLife.00994>.
13. Coffman SR, Lu J, Guo X, Zhong J, Jiang H, Broitman-Maduro G, Li W-X, Lu R, Maduro M, Ding S-W. 2017. *Caenorhabditis elegans* RIG-I homolog mediates antiviral RNA interference downstream of Dicer-dependent biogenesis of viral small interfering RNAs. *mBio* 8:e00264-17. <https://doi.org/10.1128/mBio.00264-17>.
14. Gammon DB, Ishidate T, Li L, Gu W, Silverman N, Mello CC. 2017. The antiviral RNA interference response provides resistance to lethal arbovirus infection and vertical transmission in *Caenorhabditis elegans*. *Curr Biol* 27:795–806. <https://doi.org/10.1016/j.cub.2017.02.004>.
15. Guo X, Zhang R, Wang J, Ding S-W, Lu R. 2013. Homologous RIG-I-like helicase proteins direct RNAi-mediated antiviral immunity in *C. elegans* by distinct mechanisms. *Proc Natl Acad Sci U S A* 110:16085–16090. <https://doi.org/10.1073/pnas.1307453110>.
16. Lu R, Yigit E, Li W-X, Ding S-W. 2009. An RIG-I-like RNA helicase mediates antiviral RNAi downstream of viral siRNA biogenesis in *Caenorhabditis elegans*. *PLoS Pathog* 5:e1000286. <https://doi.org/10.1371/journal.ppat.1000286>.
17. Félix M-A, Ashe A, Piffaretti J, Wu G, Nuez I, BÉlicard T, Jiang Y, Zhao G, Franz CJ, Goldstein LD, Sanroman M, Miska EA, Wang D. 2011. Natural and experimental infection of *Caenorhabditis* nematodes by novel viruses related to nodaviruses. *PLoS Biol* 9:e1000586. <https://doi.org/10.1371/journal.pbio.1000586>.
18. Yuan W, Zhou Y, Fan Y, Tao YJ, Zhong W. 2018. Orsay  $\delta$  protein is required for nonlytic viral egress. *J Virol* 92:e00745-18. <https://doi.org/10.1128/JVI.00745-18>.
19. Tanguy M, Véron L, Stempor P, Ahringer J, Sarkies P, Miska EA. 2017. An alternative STAT signaling pathway acts in viral immunity in *Caenorhabditis elegans*. *mBio* 8:e00924-17. <https://doi.org/10.1128/mBio.00924-17>.
20. Bakowski MA, Desjardins CA, Smelkinson MG, Dunbar TL, Dunbar TA, Lopez-Moyado IF, Rifkin SA, Cuomo CA, Troemel ER. 2014. Ubiquitin-mediated response to microsporidia and virus infection in *C. elegans*. *PLoS Pathog* 10:e1004200. <https://doi.org/10.1371/journal.ppat.1004200>.
21. Chen K, Franz CJ, Jiang H, Jiang Y, Wang D. 2017. An evolutionarily conserved transcriptional response to viral infection in *Caenorhabditis* nematodes. *BMC Genomics* 18:303. <https://doi.org/10.1186/s12864-017-3689-3>.
22. Reddy KC, Dror T, Underwood RS, Osman GA, Elder CR, Desjardins CA, Cuomo CA, Barkoulas M, Troemel ER. 2019. Antagonistic paralogs control a switch between growth and pathogen resistance in *C. elegans*. *PLoS Pathog* 15:e1007528. <https://doi.org/10.1371/journal.ppat.1007528>.
23. Troemel ER, Félix M-A, Whiteman NK, Barrière A, Ausubel FM. 2008. Microsporidia are natural intracellular parasites of the nematode *Caenorhabditis elegans*. *PLoS Biol* 6:2736–2752. <https://doi.org/10.1371/journal.pbio.0060309>.
24. Reddy KC, Dror T, Sowa JN, Panek J, Chen K, Lim ES, Wang D, Troemel ER. 2017. An intracellular pathogen response pathway promotes proteostasis in *C. elegans*. *Curr Biol* 27:3544–3553. <https://doi.org/10.1016/j.cub.2017.10.009>.
25. Leyva-Díaz E, Stefanakis N, Carrera I, Glenwinkel L, Wang G, Driscoll M, Hobert O. 2017. Silencing of repetitive DNA is controlled by a member of an unusual *Caenorhabditis elegans* gene family. *Genetics* 207:529–545. <https://doi.org/10.1534/genetics.117.300134>.
26. Sowa JN, Jiang H, Somasundaram L, Xu G, Wang D, Troemel ER. 2019. The *C. elegans* RIG-I homolog *drh-1* mediates the intracellular pathogen response upon viral infection. *bioRxiv* <https://doi.org/10.1101/707141>.
27. Guo Z, Li Y, Ding S-W. 2019. Small RNA-based antimicrobial immunity. *Nat Rev Immunol* 19:31–44. <https://doi.org/10.1038/s41577-018-0071-x>.
28. Parrish S, Fire A. 2001. Distinct roles for RDE-1 and RDE-4 during RNA interference in *Caenorhabditis elegans*. *RNA* 7:1397–1402.
29. Billi AC, Fischer SEJ, Kim JK. 7 May 2014. Endogenous RNAi pathways in *C. elegans*. In *The C. elegans Research Community, WormBook* (ed), WormBook. <https://doi.org/10.1895/wormbook.1.170.1>.
30. Jiang H, Chen K, Sandoval LE, Leung C, Wang D. 2017. An evolutionarily conserved pathway essential for Orsay virus infection of *Caenorhabditis elegans*. *mBio* 8:e00940-17. <https://doi.org/10.1128/mBio.00940-17>.
31. Jiang H, Wang D. 2018. The microbial zoo in the *C. elegans* intestine: bacteria, fungi and viruses. *Viruses* 10:E85. <https://doi.org/10.3390/v10020085>.
32. Kim DH, Ewbank JJ. 14 August 2018. Signaling in the innate immune response. In *The C. elegans Research Community, WormBook* (ed), WormBook. <https://doi.org/10.1895/wormbook.1.83.2>.
33. Leggewie M, Schnettler E. 2018. RNAi-mediated antiviral immunity in insects and their possible application. *Curr Opin Virol* 32:108–114. <https://doi.org/10.1016/j.coviro.2018.10.004>.
34. Xu J, Cherry S. 2014. Viruses and antiviral immunity in *Drosophila*. *Dev Comp Immunol* 42:67–84. <https://doi.org/10.1016/j.dci.2013.05.002>.
35. Zugasti O, Bose N, Squiban B, Belouigne J, Kurz CL, Schroeder FC, Pujol N, Ewbank JJ. 2014. Activation of a G protein-coupled receptor by its endogenous ligand triggers the innate immune response of *Caenorhabditis elegans*. *Nat Immunol* 15:833–838. <https://doi.org/10.1038/ni.2957>.
36. Reinke AW, Balla KM, Bennett EJ, Troemel ER. 2017. Identification of microsporidia host-exposed proteins reveals a repertoire of rapidly evolving proteins. *Nat Commun* 8:14023. <https://doi.org/10.1038/ncomms14023>.
37. Dierker K, Polanowska J, Omi S, Engelmann I, Gut M, Lembo F, Ewbank JJ, Pujol N. 2011. Unusual regulation of a STAT protein by an SLC6 family transporter in *C. elegans* epidermal innate immunity. *Cell Host Microbe* 9:425–435. <https://doi.org/10.1016/j.chom.2011.04.011>.
38. Schneider WM, Chevillotte MD, Rice CM. 2014. Interferon-stimulated genes: a complex web of host defenses. *Annu Rev Immunol* 32:513–545. <https://doi.org/10.1146/annurev-immunol-032713-120231>.
39. Wang Y, Levy DE. 2006. *C. elegans* STAT cooperates with DAF-7/TGF- $\beta$  signaling to repress Dauer formation. *Curr Biol* 16:89–94. <https://doi.org/10.1016/j.cub.2005.11.061>.
40. Deddouche S, Matt N, Budd A, Mueller S, Kemp C, Galiana-Arnoux D, Dostert C, Antoniewski C, Hoffmann JA, Imler J-L. 2008. The DExH/D-box helicase Dicer-2 mediates the induction of antiviral activity in *Drosophila*. *Nat Immunol* 9:1425–1432. <https://doi.org/10.1038/ni.1664>.
41. Paradkar PN, Duchemin J-B, Voysey R, Walker PJ. 2014. Dicer-2-dependent activation of *Culex* Vago occurs via the TRAF-Rel2 signaling pathway. *PLoS Negl Trop Dis* 8:e2823. <https://doi.org/10.1371/journal.pntd.0002823>.
42. Brehm A, Liu Y, Sheikh A, Marrero B, Omoyinmi E, Zhou Q, Montealegre G, Biancotto A, Reinhardt A, Almeida de Jesus A, Pelletier M, Tsai WL, Remmers EF, Kardava L, Hill S, Kim H, Lachmann HJ, Megarbane A, Chae JJ, Brady J, Castillo RD, Brown D, Casano AV, Gao L, Chapelle D, Huang Y, Stone D, Chen Y, Sotzny F, Lee C-CR, Kastner DL, Torrello A, Zlotogorski A, Moir S, Gadina M, McCoy P, Wesley R, Rother K, Rother K, Hildebrand PW, Brogan P, Krüger E, Aksentjevich I, Goldbach-Mansky R. 2015. Additive loss-of-function proteasome subunit mutations in CANDL/PRAAS patients promote type I IFN production. *J Clin Invest* 125:4196–4211. <https://doi.org/10.1172/JCI81260>.
43. Kretschmer S, Lee-Kirsch MA. 2017. Type I interferon-mediated autoinflammation and autoimmunity. *Curr Opin Immunol* 49:96–102. <https://doi.org/10.1016/j.coi.2017.09.003>.
44. Uggetti C, Lepelley A, Crow YJ. 2019. Self-awareness: nucleic acid-driven inflammation and the type I interferonopathies. *Annu Rev Immunol* 37:247–267. <https://doi.org/10.1146/annurev-immunol-042718-041257>.
45. Brenner S. 1974. The genetics of *Caenorhabditis elegans*. *Genetics* 77:71–94.
46. Arribere JA, Bell RT, Fu BXH, Artiles KL, Hartman PS, Fire AZ. 2014. Efficient marker-free recovery of custom genetic modifications with CRISPR/Cas9 in *Caenorhabditis elegans*. *Genetics* 198:837–846. <https://doi.org/10.1534/genetics.114.169730>.
47. Estes KA, Szumowski SC, Troemel ER. 2011. Non-lytic, actin-based exit of intracellular parasites from *C. elegans* intestinal cells. *PLoS Pathog* 7:e1002227. <https://doi.org/10.1371/journal.ppat.1002227>.
48. Pfaffl MW. 2001. A new mathematical model for relative quantification in real-time RT-PCR. *Nucleic Acids Res* 29:e45. <https://doi.org/10.1093/nar/29.9.e45>.
49. Andrews S. 2010. FastQC: a quality control tool for high throughput sequence data. Java. Babraham Bioinformatics, Cambridge, United Kingdom.
50. Bolger AM, Lohse M, Usadel B. 2014. Trimmomatic: a flexible trimmer for

- Illumina sequence data. *Bioinformatics* 30:2114–2120. <https://doi.org/10.1093/bioinformatics/btu170>.
51. Zerbino DR, Achuthan P, Akanni W, Amode MR, Barrell D, Bhai J, Billis K, Cummins C, Gall A, Girón CG, Gil L, Gordon L, Haggerty L, Haskell E, Hourlier T, Izuogu OG, Janacek SH, Juettemann T, To JK, Laird MR, Lavidas I, Liu Z, Loveland JE, Maurel T, McLaren W, Moore B, Mudge J, Murphy DN, Newman V, Nuhn M, Ogeh D, Ong CK, Parker A, Patricio M, Riat HS, Schuilenburg H, Sheppard D, Sparrow H, Taylor K, Thormann A, Vullo A, Walts B, Zadissa A, Frankish A, Hunt SE, Kostadima M, Langridge N, Martin FJ, Muffato M, Perry E, et al. 2018. Ensembl 2018. *Nucleic Acids Res* 46:D754–D761. <https://doi.org/10.1093/nar/gkx1098>.
  52. Dobin A, Davis CA, Schlesinger F, Drenkow J, Zaleski C, Jha S, Batut P, Chaisson M, Gingeras TR. 2013. STAR: ultrafast universal RNA-seq aligner. *Bioinformatics* 29:15–21. <https://doi.org/10.1093/bioinformatics/bts635>.
  53. Li B, Dewey CN. 2011. RSEM: accurate transcript quantification from RNA-Seq data with or without a reference genome. *BMC Bioinformatics* 12:323. <https://doi.org/10.1186/1471-2105-12-323>.
  54. Frankish A, Diekhans M, Ferreira A-M, Johnson R, Jungreis I, Loveland J, Mudge JM, Sisu C, Wright J, Armstrong J, Barnes I, Berry A, Bignell A, Carbonell Sala S, Chrast J, Cunningham F, Di Domenico T, Donaldson S, Fiddes IT, García Girón C, Gonzalez JM, Grego T, Hardy M, Hourlier T, Hunt T, Izuogu OG, Lagarde J, Martin FJ, Martínez L, Mohanan S, Muir P, Navarro FCP, Parker A, Pei B, Pozo F, Ruffier M, Schmitt BM, Stapleton E, Suner M-M, Sycheva I, Uszczynska-Ratajczak B, Xu J, Yates A, Zerbino D, Zhang Y, Aken B, Choudhary JS, Gerstein M, Guigó R, Hubbard TJP, et al. 2019. GENCODE reference annotation for the human and mouse genomes. *Nucleic Acids Res* 47:D766–D773. <https://doi.org/10.1093/nar/gky955>.
  55. Robinson MD, McCarthy DJ, Smyth GK. 2010. edgeR: a Bioconductor package for differential expression analysis of digital gene expression data. *Bioinformatics* 26:139–140. <https://doi.org/10.1093/bioinformatics/btp616>.
  56. Ritchie ME, Phipson B, Wu D, Hu Y, Law CW, Shi W, Smyth GK. 2015. limma powers differential expression analyses for RNA-sequencing and microarray studies. *Nucleic Acids Res* 43:e47. <https://doi.org/10.1093/nar/gkv007>.
  57. Law CW, Chen Y, Shi W, Smyth GK. 2014. voom: precision weights unlock linear model analysis tools for RNA-seq read counts. *Genome Biol* 15:R29. <https://doi.org/10.1186/gb-2014-15-2-r29>.
  58. Robinson MD, Oshlack A. 2010. A scaling normalization method for differential expression analysis of RNA-seq data. *Genome Biol* 11:R25. <https://doi.org/10.1186/gb-2010-11-3-r25>.
  59. Benjamini Y, Hochberg Y. 1995. Controlling the false discovery rate: a practical and powerful approach to multiple testing. *J R Stat Soc Series B Stat Methodol* 57:289–300. <https://doi.org/10.1111/j.2517-6161.1995.tb02031.x>.